Electrocatalysis (2017) 8:245–251
DOI 10.1007/s12678-017-0360-3

ORIGINAL RESEARCH

PtRu Nanoparticles Supported on Phosphorous-Doped Carbon as Electrocatalysts for Methanol Electro-Oxidation

Viviane Santos Pereira[1] · **Julio C. M. da Silva**[1] · **Almir Oliveira Neto**[1] · **Estevam V. Spinacé**[1]

Published online: 24 February 2017

Abstract P-doped carbon was prepared by thermal treatment of commercial carbon Vulcan XC72 with H_3PO_4 at 800 °C. PtRu nanoparticles were supported on carbon Vulcan XC72 (C) and on P-doped carbon (P-C) using an alcohol reduction process. The obtained materials were characterized by energy-dispersive X-ray spectroscopy, Raman spectroscopy, X-ray diffraction, transmission electron microscopy, and cyclic voltammetry. The performance of the electrocatalyst was evaluated for methanol electro-oxidation. The intensities of D-band and G-band of Raman spectra were different for P-doped carbon and carbon Vulcan XC72. X-ray diffraction of PtRu/C electrocatalyst showed that Pt face-centered cubic phase and Ru amorphous phase coexist in this material, while for PtRu/P-C electrocatalyst, it was observed the presence of PtRu alloy and Ru hexagonal close-packed phases. The use of P-doped carbon as support for PtRu nanoparticles improves the methanol electro-oxidation. This increase of activity could be attributed to a decrease of average nanoparticle sizes and/or more active Pt and Ru species resulting from metal-support interactions.

Keywords P-doped carbon · Platinum · Ruthenium · Nanoparticles · Electrocatalysts · Methanol

Introduction

Fuel cells convert chemical energy directly into electrical energy with high efficiency; however, the use of hydrogen as a fuel still presents problems, principally with its storage [1]. In this sense, fuel cells employing liquid fuels as combustible are very attractive as power source for portable and mobile applications [2]. Methanol is a liquid fuel that can be produced from fossil or renewable resources [3, 4], and its use in fuel cell (direct methanol fuel cell (DMFC)) has been aroused great interest. PtRu nanoparticles supported on carbon (PtRu/C) has been proved to be the most effective catalyst for methanol electro-oxidation; on the other hand, its sluggish kinetics should be improved to produced highly efficient DMFCs [5]. The performances of PtRu/C electrocatalysts have been shown to be strongly dependent on the method of preparation and on the characteristics of the carbon support. Thus, many studies have been reported on the synthesis of heteroatom-doped carbons and their use as supports to prepare Pt/C and PtRu/C electrocatalysts for methanol electro-oxidation [6, 7]. Nitrogen-doped carbons have been the most studied material as support to prepare electrocatalysts for DMFC. The increase of performance of these materials has been attributed to a modification of nucleation and growth kinetics during nanoparticle deposition resulting in smaller particle sizes and increased particle dispersion. Also, increased support-nanoparticle interaction results in enhanced durability and modification of electronic structure enhancing the catalytic activity [6, 8].

Lately, the use of phosphorous species in the synthesis of Pt and PtRu electrocatalysts has been described in the literature. Daimon and Kurobe [9] prepared PtRu nanoparticles supported on carbon support by a polyol process in the presence of non-metallic elements like N, P, and S, where different sources of phosphorous like hypophosphite, hydrogenphosphite, dihydrogenphosphate were added in the synthesis process. It was observed that the addition of non-metallic elements reduced the size of PtRu catalyst particle and improved the catalytic performance for methanol electro-oxidation, being P the most effective additive on the particle size reduction. PtRuP/C

✉ Estevam V. Spinacé
espinace@ipen.br

[1] Instituto de Pesquisas Energéticas e Nucleares IPEN-CNEN/SP, Av. Prof. Lineu Prestes, 2242—Cidade Universitária, São Paulo, SP, Brazil

[10] and PtRuNiP/C [11] electrocatalysts were also prepared by different methodologies adding hypophosphite as phosphorous source in the synthesis process. The obtained materials showed good activity for methanol electro-oxidation. Chang et al. [12] showed that the deposition of Pt on Ni_2P/C enhanced the activity and durability of the resulting Pt-Ni_2P/C electrocatalyst for methanol electro-oxidation. Non-supported electrocatalysts like porous Pt-Ni-P [13] and dendritic Pt-Ni-P [14] also showed good performances for methanol electro-oxidation. On the other hand, the use of phosphorous-doped carbons as support to prepare electrocatalysts for methanol electro-oxidation has been little explored. Liu et al. [15] prepared Pt supported on phosphorous-doped carbon nanotube as anode for DMFC indicating a highly potential application of this catalyst. Song et al. [16] prepared Pt nanoparticles incorporated into phosphorous-doped ordered mesoporous carbons and described that this may be an excellent anode catalyst for DMFC.

Despite these good results, the preparation of PtRu nanoparticles supported on phosphorous-doped carbon (PtRu/P-C) has not been described in the literature. In this work, P-doped carbon was prepared by thermal treatment of carbon Vulcan XC72 with H_3PO_4 and used as support for Pt and PtRu nanoparticles. The resulting Pt/P-C and PtRu/P-C electrocatalysts were tested for methanol electro-oxidation.

Materials and Methods

Synthesis of P-Doped Carbon

P-doped carbon was prepared by a procedure similar to described in the references [17, 18]; in this process, 200 mg of carbon Vulcan XC72 was dispersed in 5 mL of water and 160 mg of phosphoric acid was added. The resulting mixture was stirred for 20 min and dried at 80 °C for 2 h. The obtained paste mixture was heated under argon flow (100 mL min^{-1}) in a tube furnace from room temperature to 800 °C (10 °C min^{-1}) and maintained for 2 h. Finally, the solid was cooled under argon flow to room temperature, washed with excess of water, and dried at 70 °C for 2 h.

Preparation of Pt and PtRu Electrocatalysts

PtRu/C eletrocatalysts (Pt/Ru atomic ratio 50:50) were prepared by an alcohol reduction process [19] with 20 wt% of metal loading using $H_2PtCl_6{\cdot}H_2O$ (Aldrich) and $RuCl_3{\cdot}xH_2O$ (Aldrich) as metal sources, ethylene glycol (Merck) as solvent and reducing agent, and carbon Vulcan XC72 or P-doped carbon as supports. In a typical procedure, the metal sources were dissolved in ethylene glycol/water (75/25, *v*/*v*) and the carbon support was added. The resulting mixtures were treated in an ultrasound bath and were refluxed for 3 h under open atmosphere. The mixtures were filtered and the solids washed with water and dried at 70 °C for 2 h.

Characterizations

Raman measurements of carbon supports were performed on LAMULT (Xplora) da Horiba spectrometer with a laser wavelength of 532 nm. The spectra were obtained in triplicate for each sample in the region between 1200 and 1700 cm^{-1}.

The Pt/Ru atomic ratios of the electrocatalysts were obtained by EDAX analysis using a scanning electron microscope Philips XL30 with a 20 keV electron beam and equipped with EDAX DX-4 microanalyzer.

The X-ray diffraction analyses were performed using a Rigaku diffractometer model Miniflex II using Cu Kα radiation source (l = 0.15406 nm). The diffractograms were recorded in the range of 2θ between 20° and 90° with a step size of 0.05° and a scan time of 2 s per step.

Transmission electron microscopy (TEM) was carried out using a JEOL JEM-2100 electron microscope operated at 200 kV. The average particle sizes were determined by measuring of 200 nanoparticles from micrographs using Image Tool Software.

Electrochemical Measurements

The electrochemical experiments were performed using Metrohm Autolab potentiostat. A three-electrode cell system with an ultrathin vitreous carbon layer previously polished was used as work electrode, a platinum plate as counter electrode, and hydrogen electrode (HRE) as reference. An aliquot of ultrasonicated catalytic ink containing water (900 μL), isopropyl alcohol (100 μL), Nafion solution 5% (20 μL), and the catalytic powder (1 mg) was dropped onto the electrode surface, and it was dried in air. Cyclic voltammetry (CV) and chronoamperometry (CA) tests were carried out to characterize and test the electrocatalytic activity of the as-prepared materials. CV was performed in 0.5 mol L^{-1} H_2SO_4 at a scan rate of 50 mV s^{-1}. CA experiments were carried out in 1 mol L^{-1} of methanol in 0.5 mol L^{-1} H_2SO_4 at 0.5 V (vs. RHE) for 1800 s. For comparative purposes, a commercial Pt/C from BASF (20 wt% Pt on Vulcan XC72, Lot #F0381022) and PtRu/C from BASF (20 wt% PtRu on Vulcan XC72, Pt/Ru atomic ratio of 1:1, Lot #C1180928) were used.

Results and Discussion

Initially, the carbon Vulcan XC72 was treated at 800 °C under argon atmosphere to eliminate any impurities present. Further, it was treated in the presence of H_3PO_4 at 800 °C in an argon atmosphere. The Raman spectra were used to confirm the structure of P-doped carbon (Fig. 1). The ratio of intensities

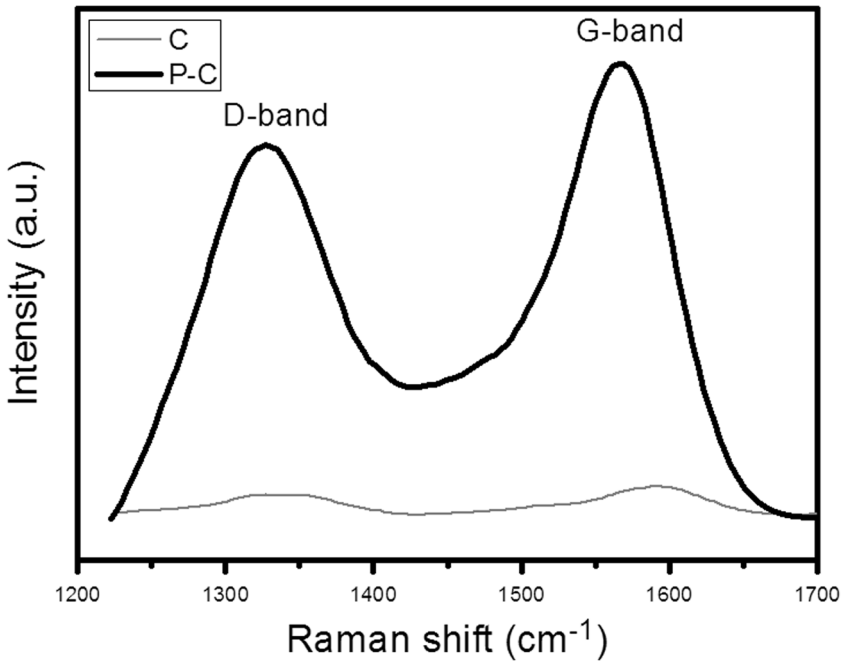

Fig. 1 Raman spectra of carbon Vulcan XC72 (C) and phosphorous-doped carbon (P-C)

of D-band (1340 cm^{-1}) and G-band (1590 cm^{-1}) was used to measure the carbon disorder caused by H_3PO_4 activation [20]. The I_D/I_G ratios of P-doped carbons are greater than the ones observed for undoped carbons [16, 17, 20]. As expected, the I_D/I_G ratio of the prepared P-doped carbon (0.81 ± 0.02) was greater than the one of the starting material Vulcan XC72 (0.71 ± 0.04). The H_3PO_4 treatment could also promote an increase of pore volume, pore size distribution, and specific surface area as already observed in similar studies [16, 20]. The XPS P2p spectra of P-doped carbons prepared in a similar way [17, 18] showed the presence of P-C bonding, which is a result of bond cleavage reactions and the formation of cross-links between phosphoric acid and carbon-containing fragments during activation. The presence of P-O bondings was also observed in the XPS spectra, and it was attributed to the presence of phosphate species that were bonded to carbon through the oxygen atom forming P-O-C bonding [17, 18].

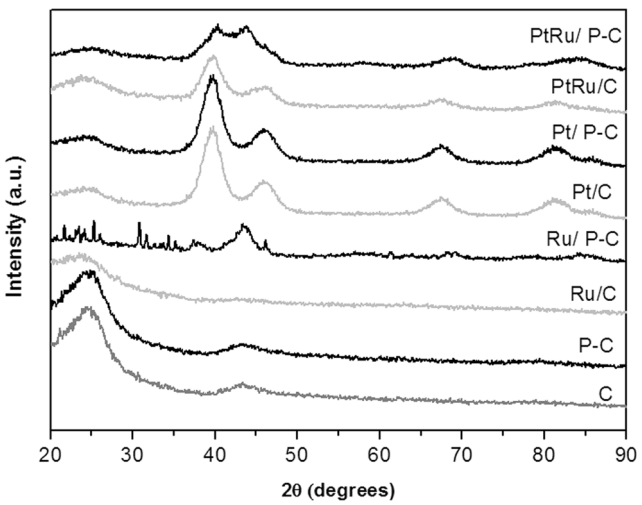

Fig. 2 X-ray diffraction of carbon support, P-doped carbon support, and Ru/C, Ru/P-C, Pt/C, Pt/P-C, PtRu/C, and PtRu/P-C electrocatalysts

The X-ray diffractograms of Pt, Ru, and PtRu nanoparticles supported on Vulcan XC72 (Pt/C, Ru/C, and PtRu/C) and on P-doped carbon (Pt/P-C, Ru/P-C, and PtRu/P-C) are shown in Fig. 2. For Vulcan XC72 support (C) and P-doped carbons (P-C), it was observed two broad peaks at about 2θ = 25° and 43° associated to the (002) and (004) planes of hexagonal structure and characteristic of amorphous carbon [21]. The XRD diffraction of Ru/C electrocatalyst only showed the peaks characteristic of amorphous carbon; no peaks of crystalline Ru metallic or Ru oxide phases were observed, suggesting that Ru was present as an amorphous phase. On the other hand, X-ray diffractogram of Ru/P-C electrocatalyst showed many peaks that were compared to ICDD database for metallic Ru, ruthenium oxides, ruthenium phosphides [22, 23], and ruthenium phosphates [24]. However, the broadness and overlapping of the diffraction peaks make the analysis difficult. As a result, only a hexagonal closed packed (hcp) structure typical for metallic Ru could be identified by the broad peak at about 2θ = 44°, which is the most intense reflection, and by the additional peaks at about 38.4°, 69.4°, and 84.7° [25]. The remaining peaks could not be exactly matched with other phases containing Ru, P, and/or O. Nevertheless, the presence of phases containing these elements cannot be discarded. X-ray diffractograms of Pt/C and Pt/P-C electrocatalysts showed

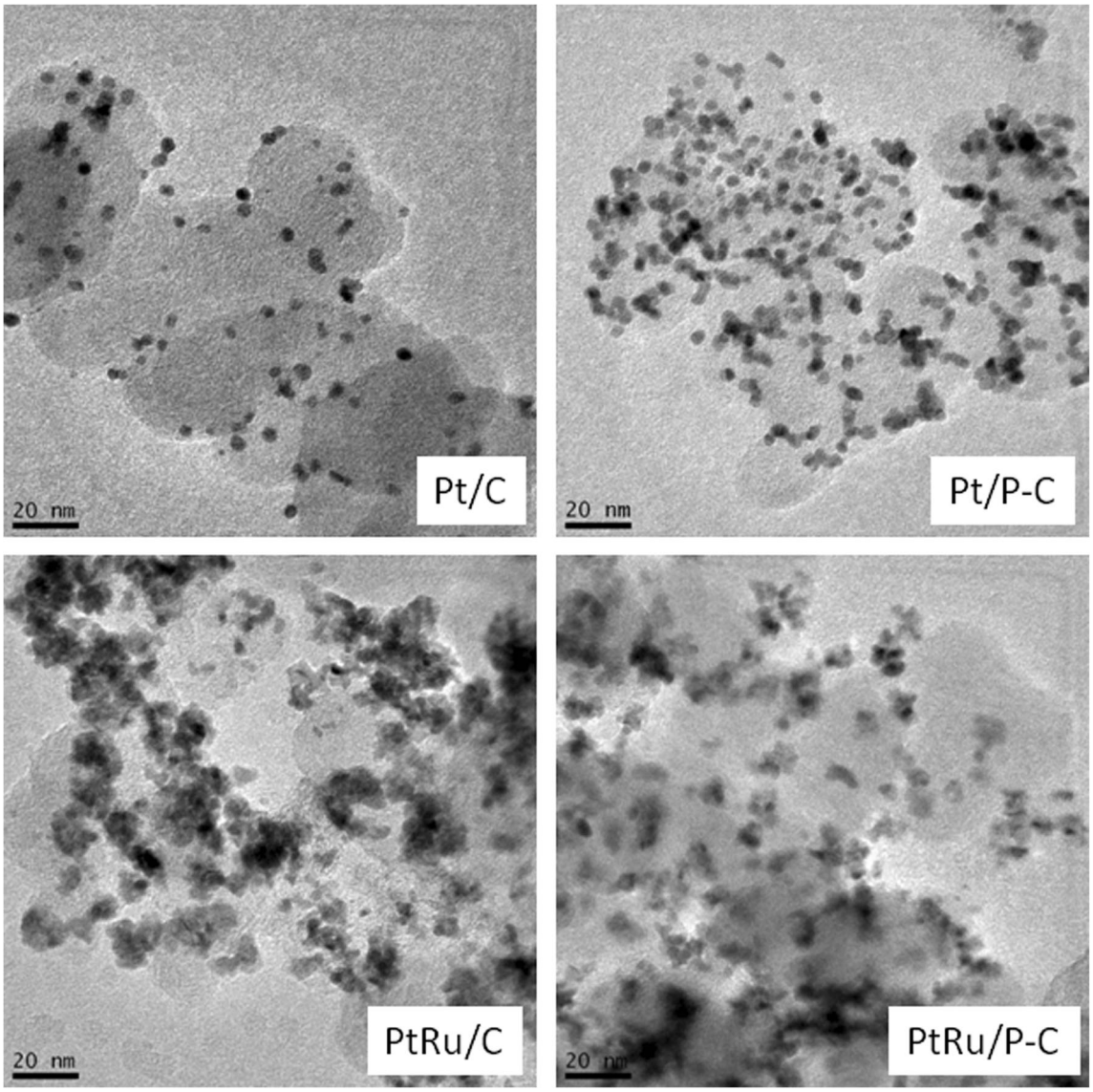

Fig. 3 Transmission electron micrographs of Pt/C, Pt/P-C, PtRu/C, and PtRu/P-C electrocatalyts

the typical peaks of Pt face-centered cubic (cfc) structure showing peaks at approximately 2θ = 39°, 46°, 67°, and 81° that correspond to (111), (200), (220), and (311) planes, respectively [19]. PtRu/C electrocatalyst also showed the characteristic peaks of Pt (fcc) phase, and they were not shifted to higher angles indicating no PtRu alloy formation [19]. No peaks of Ru metallic or Ru oxide phases were observed suggesting that Ru was present as an amorphous phase, since in the EDX analysis of this sample, the Pt/Ru experimental atomic ratio was 52:48 which is very close to the nominal ratio 50:50. Interestingly, X-ray diffractogram of PtRu/P-C electrocatalyts showed the characteristic peaks of Pt (fcc) phase; however, they were shifted to higher angles indicating a PtRu alloy formation [19]. It was also observed the presence of a peak at about 2θ = 44°, which is characteristic of Ru (hcp) phase [25]. In this case, a Pt/Ru atomic ratio (45:55) similar to the nominal value was also obtained. Curiously, comparing the materials containing Ru (Ru/C with Ru/P-C and PtRu/C with PtRu/P-C), it can be seen that when carbon Vulcan XC72 (C) was used as support, diffraction peaks of crystalline Ru phases were not observed, while for materials prepared using P-doped carbon (P-C), the presence of crystalline Ru phases was observed.

The transmission electron micrographs of Pt/C, Pt/P-C, PtRu/C, and PtRu/P-C electrocatalysts are shown in Fig. 3. For Pt/C electrocatalyst, it was observed a good distribution of Pt nanoparticles on the carbon support and an average particle size of 4.2 nm, while for Pt/P-C electrocatalyst, the nanoparticles are also well dispersed and in a smaller average size (3.8 nm). A similar feature was observed for PtRu/C (3.7 nm) and PtRu/P-C (2.9 nm) electrocatalysts. It was already described that the addition of phosphorous sources on the

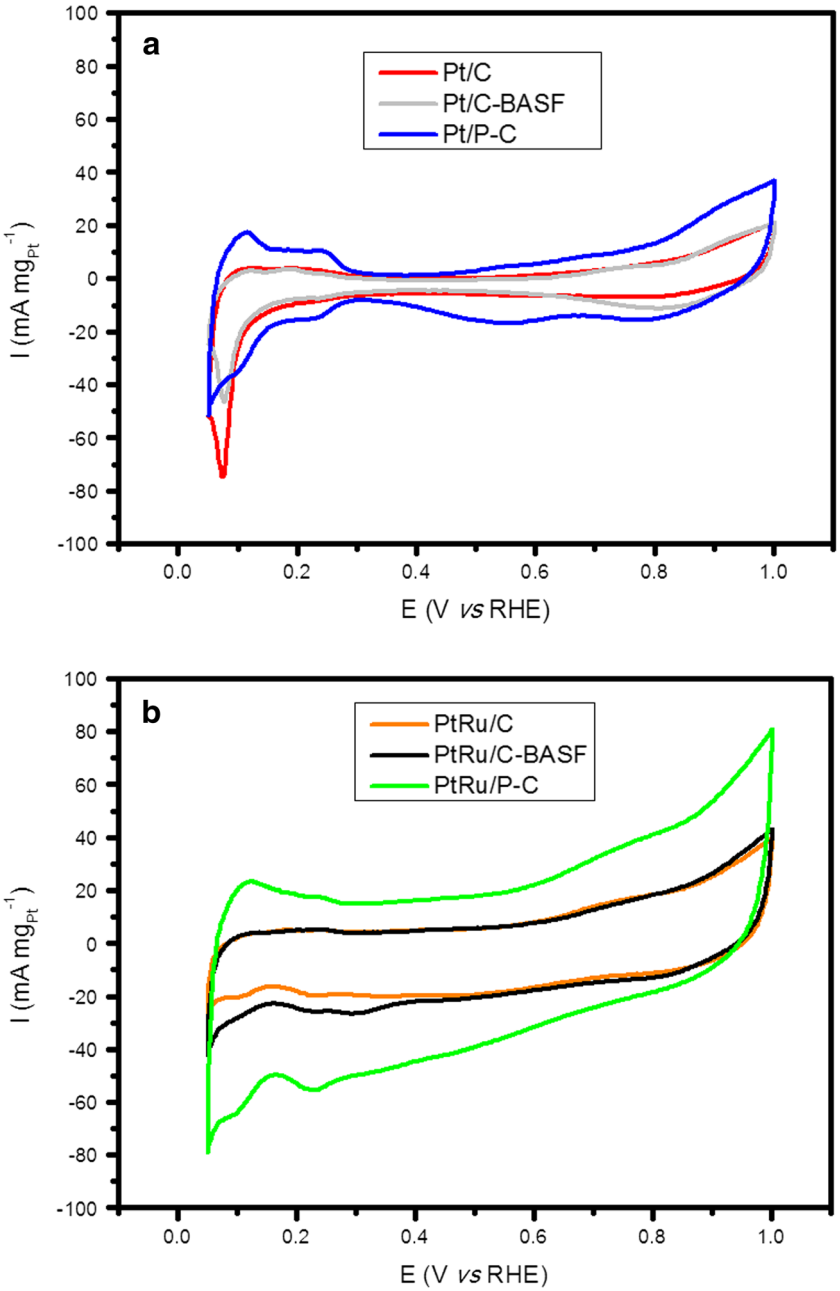

Fig. 4 Cyclic voltammograms of **a** Pt/C, Pt/P-C, and commercial Pt/C and **b** PtRu/C and PtRu/P-C and commercial PtRu/C electrocatalysts in solution of 0.5 mol L^{-1} H_2SO_4 at 50 mV s^{-1}

synthesis of PtRu/C electrocatalysts [9] and the preparation of Pt/C using phosphorus-doped ordered mesoporous carbons as support decreased the average particle sizes [15].

The CVs of Pt/C, Pt/P-C, PtRu/C, PtRu/P-C, and commercial electrocatalysts in 0.5 mol L^{-1} of H_2SO_4 at 50 mV s^{-1} are shown in Fig. 4a, b. The CV of Pt/C is in accordance to expected electrocatalyst profile in acid media showing the hydrogen adsorption/desorption region, double-layer region, and oxide formation region at 0.0–0.4, 0.4–0.65, and >0.65 V, respectively. The hydrogen adsorption/desorption region peak at 0.05–0.15 V was assigned to the (110)-type sites, and the peak at 0.20–0.30 V contains two contributions from (100) step sites on (111) terraces and the sites close to the steps on the (100) terraces [26, 27]. The peak features of hydrogen adsorption/desorption region of Pt/P-C electrocatalyst are different from the Pt/C electrocatalyst. The peak observed at about 0.12 V due the contribution of (110)-type sites was relatively more intense than the contribution of (100)-type sites at about 0.25 V, while for Pt/C, these contributions were similar. Furthermore, it was observed an enlargement of the double-layer region which could probably be due to phosphorous oxygen species like P-O [17, 18]. Similar features were

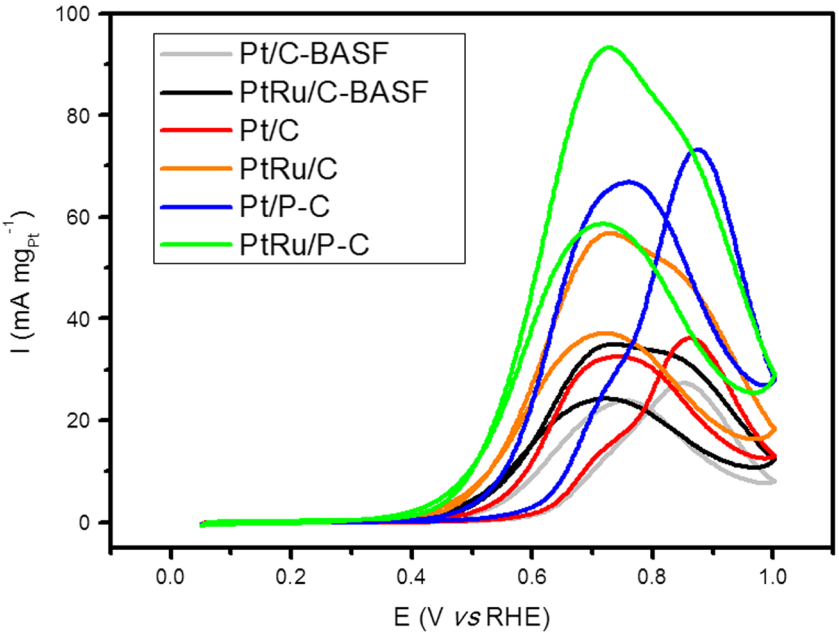

Fig. 5 Cyclic voltammograms of Pt/C, Pt/P-C, PtRu/C, and PtRu/P-C electrocatalysts in solution of 1.0 mol L^{-1} in 0.5 mol L^{-1} H_2SO_4 at 50 mV s^{-1}

seen comparing PtRu/P-C with PtRu/C electrocatalyst; in this manner, the use of P-C as support changes the features of the electrocatalyst materials.

The CVs of Pt/C, Pt/P-C, PtRu/C, and PtRu/P-C electrocatalysts at 50 mV s^{-1} scan rate in 1 mol L^{-1} methanol in 0.5 mol L^{-1} H_2SO_4 are shown in Fig. 5. The currents were normalized per gram of Pt. Pt/P-C electrocatalyst electro-oxidizes methanol at lower overpotentials than Pt/C electrocatalyst, and the current values are greater in the all potential range. As expected, using PtRu electrocatalysts, higher current density from methanol electro-oxidation was obtained in all the potential range; additionally, this material electro-oxidizes methanol at lower potential than Pt electrocatalysts; however again, the material prepared with P-C as support showed superior activity. The long-term stabilities of the electrocatalysts were examined by chronoamperometry experiments under a constant potential of 0.5 V (Fig. 6), and the results are in agreement with the order of electrocatalytic activity observed in CV tests. Furthermore, the materials show good stability. The current density from methanol electro-oxidation at the end of the experiments using PtRu/P-C was about two times higher than PtRu/C, while using Pt/P-C, the

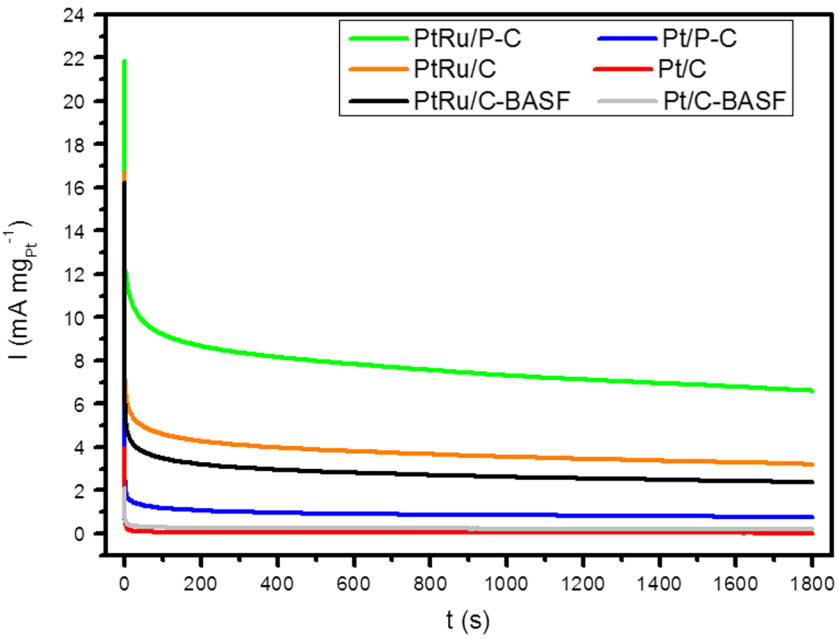

Fig. 6 Chronoamperometry curves of Pt/C, Pt/P-C, PtRu/C, and PtRu/P-C electrocatalysts in solution of 0.5 mol L^{-1} H_2SO_4 at 0.5 V

current density was about three times higher than Pt/C. Similar results were observed when compared to commercial Pt/C and PtRu/C electrocatalyts. Similar results on catalyst performances were observed for Pt nanoparticles supported on phosphorus-doped carbon nanotube [15] and on phosphorus-doped ordered mesoporous carbons for methanol electro-oxidation [16]. The increase of activity in these cases was attributed to a decrease of size and a homogeneous dispersion of the Pt nanoparticles.

The superior performance of PtRu/P-C electrocatalysts for methanol electro-oxidation when compared to PtRu/C electrocatalysts probably could be attributed to the following factors: a decrease of the nanoparticle sizes resulting from the presence of phosphorous species and/or to an increase of pore volume and specific surface area of the P-doped carbon favoring the dispersion [9, 16]. It could also be due to the presence of more active Pt and Ru species resulting from metals and P-doped carbon interactions.

Conclusions

The use of P-doped carbon as support for PtRu nanoparticles results in an increase of electrocatalytic activity for methanol electro-oxidation. PtRu/C electrocatalyst contains a mixture of Pt (fcc) nanoparticles and an amorphous Ru phase, while PtRu/P-C electrocatalyst showed the presence of PtRu alloy nanoparticles and Ru (hcp) phases. The increase of catalytic activity could be attributed to a decrease of average nanoparticle sizes and more active Pt and Ru species resulting from metal-support interactions.

Acknowledgements VSP thank CNPq for scholar fellowship and CNPq (Proc. No. 310051/2012-6) and FAPESP (Proc. No. 2014/09087-4) for financial support.

References

1. Y. Xia, Z. Yang, Y. Zhu, J. Mater, Chem. A **1**, 9365–9381 (2013)
2. X. Li, A. Faghri, J. Power Sources **226**, 223–240 (2013)
3. I. Shown, H.-C. Hsu, Y.-C. Chang, C.-H. Lin, P.K. Roy, A. Ganguly, C.-H. Wang, J.-K. Chang, C.-I. Wu, L.-C. Chen, K.-H. Chen, Nano Lett. **14**, 6097–6103 (2014)
4. M. Behrens, Angew. Chem. Int. Edit. **53**, 12022–12024 (2014)
5. F. Taufany, C.-J. Pan, F.-J. Lai, H.-L. Chou, L.S. Sarma, J. Rick, J.-M. Lin, J.-F. Lee, M.-T. Tang, B. Hwang, Chem. Eur. J. **19**, 905–915 (2013)
6. Y. Zhou, K. Neyerlin, T.S. Olson, S. Pylypenko, J. Bult, H.N. Dinh, T. Gennett, Z. Shao, R. O'Hayre, Energy Environ. Sci. **3**, 1437–1446 (2010)
7. W.J. Lee, U.N. Maiti, J.M. Lee, J. Lim, T.H. Han, S.O. Kim, Chem. Commun. **50**, 6818–6830 (2014)
8. C.E. Chan-Thaw, A. Villa, G.M. Veith, L. Prati, ChemCatChem **7**, 1338–1346 (2015)
9. H. Daimon, Y. Kurobe, Catal. Today **111**, 182–187 (2006)
10. X. Xue, J. Ge, C. Liu, W. Xing, T. Lu, Electrochem. Commun. **8**, 1280–1286 (2006)
11. Y. Ma, H. Li, H. Wang, X. Mao, V. Linkov, S. Ji, O.U. Gcilitshana, R. Wang, J. Power Sources **268**, 498–507 (2014)
12. J. Chang, L. Feng, C. Liu, W. Xing, X. Hu, Energy Environ. Sci. **7**, 1628–1632 (2014)
13. L.-X. Ding, A.-L. Wang, G.-R. Li, Z.-Q. Liu, W.-X. Zhao, C.-Y. Su, Y.-X. Tong, J. Am, Chem. Soc. **134**, 5730–5733 (2012)
14. J. Zhang, K. Li, B. Zhang, Chem. Commun. **51**, 12012–12015 (2015)
15. Z. Liu, Q. Shi, F. Peng, H. Wang, R. Zhang, H. Yu, Electrochem. Commun. **16**, 73–76 (2012)
16. P. Song, L. Zhu, X. Bo, A. Wang, G. Wang, L. Guo, Electrochim. Acta **127**, 307–314 (2014)
17. J. Wua, Z. Yang, Q. Sun, X. Li, P. Strasser, R. Yang, Electrochim. Acta **127**, 53–60 (2014)
18. Y. Wen, B. Wang, C. Huang, L. Wang, D. Hulicova-Jurcakova, Chem. Eur. J. **21**, 80–85 (2015)
19. A. Oliveira Neto, R.R. Dias, M.M. Tusi, M. Linardi, E.V. Spinacé, J. Power Sources **166**, 87–91 (2007)
20. K. Hong, L. Qie, R. Zeng, Z. Yi, W. Zhang, D. Wang, W. Yin, C. Wu, Q. Fan, W. Zhang, Y. Huang, J. Mater, Chem. A **2**, 12733–12738 (2014)
21. J. Qi, L. Jiang, S. Wang, G. Sun, Appl. Catal. B - Environ **107**, 95–103 (2011)
22. Q. Guan, C. Sun, R. Li, W. Li, Catal. Commun. **14**, 114–117 (2011)
23. H. Teller, O. Krichevski, M. Gur, A. Gedanken, A. Schechter, ACS Catal. **5**, 4260–4267 (2015)
24. H. Fukuoka, H. Imoto, T. Saito, J. Solid State Chem. **119**, 107 (1995)
25. R. Chetty, W. Xia, S. Kundu, M., Bron, T. Reinecke, W. Schuhmann, M. Muhler. Langmuir **25**, 3853–3860 (2009)
26. F.J. Vidal-Iglesias, R.M. Aran-Ais, J. Solla-Gullon, E. Herrero, J.M. Feliu, ACS Catal. **2**, 901–910 (2012)
27. R. Devivaraprasad, R. Ramesh, N. Naresh, T. Kar, R.M. Singh, M. Neergat, Langmuir **30**, 8995–9006 (2014)